applied sciences

Article

Frequency-Bounded Matching Strategy for Wideband LNA Design Utilising a Relaxed SSNM Approach

Vanya Sharma *, Patrick E. Longhi, Walter Ciccognani, Sergio Colangeli, Antonio Serino, Swati Sharma and Ernesto Limiti *

Department of Electronics Engineering, University of Rome Tor Vergata, 00133 Rome, Italy; longhi@ing.uniroma2.it (P.E.L.); walter.ciccognani@uniroma2.it (W.C.); colangeli@ing.uniroma2.it (S.C.); serino@uniroma2.it (A.S.); swati.sharma@uniroma2.eu (S.S.)

* Correspondence: vanya.sharma@students.uniroma2.eu (V.S.); limiti@ing.uniroma2.it (E.L.)

Abstract

This paper proposes relaxed Simultaneous Signal and Noise Matching (SSNM) conditions to address limitations in selecting source degeneration inductors for multistage LNA design, achieved by introducing controlled mismatches at the external ports. Additionally, a novel frequency-bounded mismatch envelope is introduced to guide load termination selection based on desired IM-OM (input mismatch-output mismatch) characteristics across the operating band. Building on these concepts, a systematic, easy-to-follow strategy is presented for implementing wideband multistage low-noise amplifiers (LNAs), significantly reducing reliance on blind CAD-based optimisation. This approach is validated through a three-stage MMIC LNA prototype, fabricated using a 0.15 µm GaAs process and operating from 28 to 34 GHz. The measured results closely match the simulation, demonstrating a stable gain of 23 ± 1 dB and a noise figure of 2–2.5 dB, confirming the practical effectiveness of the proposed design approach for wideband amplifiers.

Keywords: IM-OM circles; wide-band impedance matching; mismatch regions; MMIC; LNA; GaAs pHEMTs; relaxed SSNM; frequency bounded mismatch envelope

Academic Editor: Christos Bouras

Received: 25 June 2025
Revised: 13 July 2025
Accepted: 17 July 2025
Published: 22 July 2025

Citation: Sharma, V.; Longhi, P.E.; Ciccognani, W.; Colangeli, S.; Serino, A.; Sharma, S.; Limiti, E. Frequency-Bounded Matching Strategy for Wideband LNA Design Utilising a Relaxed SSNM Approach. *Appl. Sci.* **2025**, *15*, 8148. https://doi.org/10.3390/app15158148

1. Introduction

Low-noise amplifiers (LNAs) are critical components in modern radio frequency (RF) and microwave systems, typically serving as the first active stage in a receiver chain. Their performance directly impacts the overall system noise figure (NF), making LNA design essential for applications such as automotive radar, satellite communications, electronic warfare [1–5], and biomedical applications such as ultrasound imaging systems and short-range radio, etc., at low frequency (10–1000 MHz) [6,7]. In addition to achieving an optimal trade-off between the gain and noise figure, many of these applications demand wideband operation. However, conventional LNA design methodologies often prioritise narrowband performance and rely on single-frequency matching strategies. Techniques such as source degeneration [8,9] and drain–gate feedback [10–13] have been widely adopted to bring the optimum noise and gain impedances closer together, enabling simultaneous signal and noise matching (SSNM). These feedback mechanisms help mitigate the effects of Miller capacitance (e.g., C_{gd}, C_{gs}) at high frequencies, thereby improving amplifier stability and marginally reducing noise parameters. Nevertheless, excessive feedback can degrade small-signal gain. Furthermore, achieving ideal SSNM conditions at both ports is not feasible in a single-stage amplifier, making multistage topologies more suitable. In this context, *Patrick et al.* [14] proposed a systematic approach using mismatch charts to determine appropriate feedback for each stage, while *Walter et al.* [15] introduced a method based on mismatch circles to realise SSNM. These works provide important foundations for SSNM-based design. Additionally, the influence of varying mismatch levels on gain has been explored in [16], and a graphical synthesis method on the load admittance plane has been proposed for optimised low-noise design [17]. Other efforts include multistage millimetre-wave LNAs using passive R–C–L shunt feedback to achieve wideband SNIM with high efficiency and low noise [18], although these techniques remain primarily focused on narrowband design.

To address the challenges of broadband matching, several alternative circuit topologies have been explored. Transformer-based matching [19], filter-based matching [20], and forward combining techniques [21] have demonstrated extended bandwidth. Design incorporating a series inductor at drain terminal [22] and drain to source coupling (using coupled lines) [23] also achieved flat gain and a low noise figure. While these methods are effective, they often require complex matching structures and extensive use of computer-aided design (CAD) tools, limiting the designer's ability to control mismatch levels across multiple stages. An interdisciplinary approach in reference [24] integrates linear circuit theory, noise analysis, communication theory, and soft-computing methods, using particle swarm optimisation to synthesise frequency-dependent terminations via Darlington-based networks. Similarly, reference [25] proposes an analytical formulation for source reflection in distributed matching networks to achieve broadband gain flattening.

This paper presents a systematic and practical strategy for designing wideband multistage LNAs using a relaxed SSNM framework. The approach introduces frequency-bounded mismatch regions derived from input–output mismatch circles plotted on the Smith chart. These graphical regions offer a visual and intuitive method for selecting source and load terminations across a wide frequency span, facilitating broadband impedance matching, a low noise figure, and unconditional stability, without relying on iterative CAD-based optimisation. The behaviour of input mismatch (IM) and output mismatch (OM) circles is analysed and extended into bounded regions that preserve geometric clarity while generalising their use to wideband, multistage LNA designs. To validate the proposed methodology, a three-stage monolithic microwave integrated circuit (MMIC) LNA prototype was fabricated using a 0.15 µm GaAs process, targeting the 28–34 GHz band. The general architecture of this, with various reflection coefficients and mismatches, is shown in Figure 1. Measured results demonstrate a gain of 23 ± 1 dB and a noise figure of 2–2.5 dB, closely matching simulations. These results confirm the practical effectiveness of the proposed frequency-bounded mismatch region strategy for wideband LNA design. Circuit schematics and EM simulations are performed using Keysight's Advanced Design System (ADS) software (version 2023 update 1).

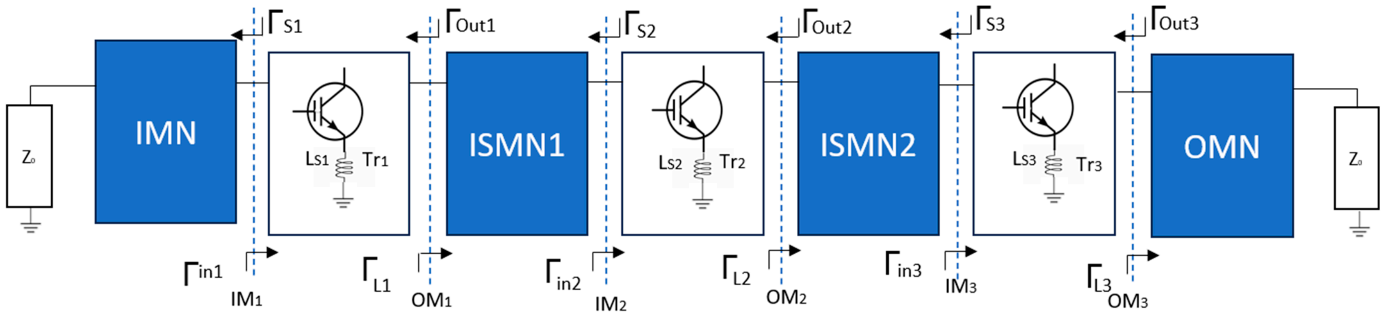

Figure 1. Detailed block architecture of the three-stage LNA.

The remainder of this paper is organised as follows: Section 2 reviews prior approaches to source degeneration and introduces the relaxed SSNM framework. Section 3 presents the concept of frequency-bounded mismatch regions. Section 4 details the proposed design methodology. Section 5 discusses measured results from the fabricated prototype, and Section 6 concludes with insights and future research directions.

2. Relaxed SSNM Conditions: Background and Choice of Source Degenerative Inductors

In traditional multistage LNA design, SSNM is achieved by enforcing strict mismatch conditions at each stage [9–11,16]. At the design frequency f_0, and assuming lossless matching networks, the following relationships are imposed:

1. Mismatch at external ports: $IM_1 = OM_n = 0$
2. Mismatch at inter-stages: $OM_n = IM_{n+1}$

This strict SSNM condition is enforced throughout a narrowband design procedure. This enforcement is used even when selecting source degeneration (L_S); an appropriate L_S is crucial in the case of LNA, as it must satisfy not only the gain–noise trade-off but also ensure signal matching.

Figure 2 shows the IM-OM pairs obtained by sweeping L_S from 0 pH to 300 pH in 10 pH steps. Both IM and OM decrease as L_S increases. For this process, the grounded FET (0 pH) yields IM = 0.891 and OM = 1.358. The geometrical stability factor (μ) remains above unity at f_0 = 31 GHz for L_S = 45 pH to 200 pH, allowing designers to choose L_S safely within the unshaded regions (for Tr2: $\mu > 1$).

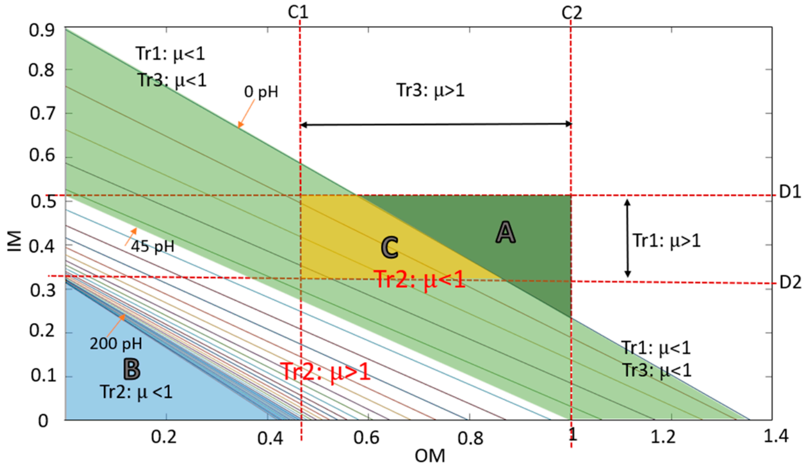

Figure 2. IM-OM vs. L_S variation chart with 10 pH steps (unshaded zones denote unconditional stable regions, allowing a visual one-shot selection of safe inductance values, shaded zones including B, C, A represent conditional stability).

The complex chart in Figure 2 is further disintegrated into smaller, more interpretable zones. Region A is unusable, as the IM-OM trace at 0 pH lies below it. The pale blue (B) and green areas (including C) correspond to conditional stable regions ($\mu < 1$). Patrick et al. [14] developed a chart-based method to select L_S values according to mismatch levels that forces the strict SSNM conditions in multistage, narrowband amplifiers. To understand the method, consider a three-stage LNA with identical biasing and transistor sizes, and assume chart shown in Figure 2 represents the second stage of the cascade network and the Y-axis equates to $OM_1 = IM_2$, while the X-axis represents $OM_2 = IM_3$. For this, we obtain an unconditional stable region for Tr1 (between D1-D2 boundaries) and Tr2 (between C1–C2). Their sole intersection region (C), where both transistors are stable, lies in the region that corresponds to $\mu < 1$ for Tr2. Any inductor value chosen in this region will come with certain limitations of source and load terminations for Tr2. This illustrates how some methods may offer limited flexibility for selecting inductor values. That limitation, however, depends on factors like transistor sizing, biasing, or technology; under different conditions, Patrick's system works effectively.

A possible solution to this problem is to relax the SSNM constraint by deliberately introducing a small mismatch at each external port. Even a mismatch of 0.1 would be a great help to reduce the limitations, and a 0.1 mismatch will equate to −20 dB reflection, which is not ideal, but still an excellent match in a practical RF system. Easing this constraint allows more flexibility in choosing appropriate source degeneration values, enabling better gain and increased stability. Figure 3 demonstrates this perfectly. Here, introducing a mismatch of 0.1 will move the IM-OM axis to a new x'-y' axis, and a mismatch of 0.2 moves it to an x''-y'' axis. This gives us an extended region to select L_S value where all transistors are within the stability margin. Also, introducing deliberate mismatches eventually leads to low inductance values. For example, in Figure 3, Point "p" in the stable region gives a low OM value compared to Figure 2, and low L_S and high OM both result in a high gain.

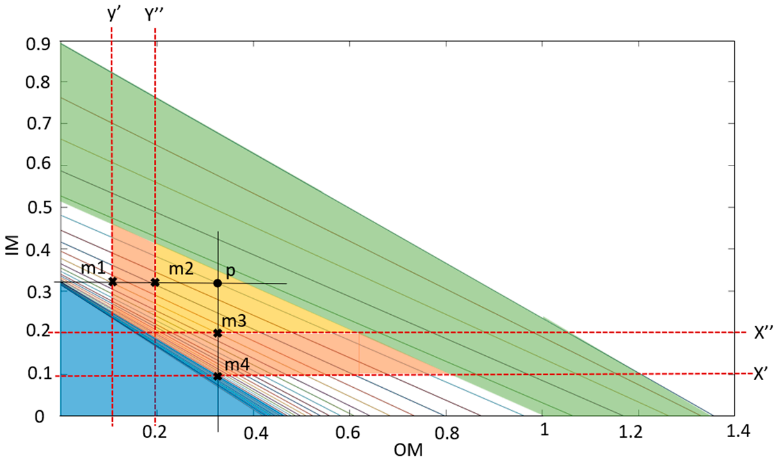

Figure 3. IM-OM vs. L_S variation (comprising the same data as in Figure 2) with an introduction of a small mismatch (X'-Y': 0.1, X''-Y'': 0.2 mismatch).

The chart shown in Figure 3 can be modified for various pairs of IM-OM values by simply shifting the axes according to the desired mismatches. Additionally, adding a mismatch does not affect NF, which depends on the source reflection coefficient (Γ_S), while mismatch at both ports is controlled only by the load reflection coefficient (Γ_L). Thus, a relaxed SSNM grants designers more freedom to assign L_S per transistor rather than being locked into strict inter-stage relationships.

Relaxed SSNM conditions for a multistage amplifier can be summarised as

1. Input external port: $IM_1 \neq 0$
2. Interstage: $OM_n = IM_{n+1}$
3. Output external port: $OM_n \neq 0$

Here, external mismatch must lie in the "good" (0–0.1) or "acceptable" (0.1–0.25) mismatch range. Even with added mismatch, the chart-based method offers little guidance for wide-band circuitry, although it is an excellent tool for initial L_S selection. In later sections, we will combine the tool with the relaxed SSNM rule to realise a wideband LNA. The next part of the paper includes developing a frequency-bounded envelope of mismatch regions on the Smith chart and defining load terminations that yield the desired mismatch combinations. This strategy will also reduce the blind dependency on software-based optimisation to obtain a wide operating band.

3. IM-OM Circles and Frequency-Bounded Mismatch Envelope

As shown in Figure 1, a two-port network such as an LNA is characterized by four reflection coefficients (Γ_S, Γ_{IN}, Γ_L and Γ_{OUT}). These coefficients determine the amount of matching at each terminal that can be calculated using IM and OM expressions. Interestingly, the reflection coefficients are interdependent and can be expressed as functions of one another.

Γ_s controls output reflection coefficients (Γ_{OUT}) through the following relation:

$$\Gamma_{OUT} = \frac{(S_{22} - \Gamma_S.\Delta)}{(1 - \Gamma_S.S_{11})} = f([S], \Gamma_S) \tag{1}$$

Similarly, Γ_L influences the input reflection coefficient (Γ_{in}) as:

$$\Gamma_{in} = \frac{(S_{11} - \Gamma_L.\Delta)}{(1 - \Gamma_L.S_{22})} = f([S], \Gamma_L) \tag{2}$$

From these equations, it follows that knowing one reflection coefficient from each side of the device is sufficient to determine all four, assuming the known values are independent.

The mismatch at each port can be computed using the equations of OM and IM as follows [12]:

$$OM = \left| \frac{\Gamma_L - {\Gamma_{out}}^*}{1 - \Gamma_L.\Gamma_{OUT}} \right| \tag{3}$$

$$OM = f(\Gamma_L, \Gamma_{OUT}) = f(\Gamma_S, [S], \Gamma_L) \tag{4}$$

And

$$IM = \left| \frac{\Gamma_S - {\Gamma_{in}}^*}{1 - \Gamma_S.\Gamma_{in}} \right| \tag{5}$$

$$IM = f(\Gamma_S, \Gamma_{in}) = f(\Gamma_S, [S], \Gamma_L) \tag{6}$$

From Equations (1)–(6), it is evident that IM and OM are mutually dependent. That is, knowledge of one can inform the other, given the appropriate device parameters. *Walter et al.* [12] first formalised these relationships and introduced a set of equations to graphically represent mismatch through IM-OM circles. In this work, we will be summarizing the behaviour of these circles and further extend the concept to derive a frequency-bounded mismatch region on the Smith chart.

3.1. IM-OM Circles for a Single Frequency Point

To illustrate the behaviour of mismatch at a single frequency point, we analyse the IM-OM circles using the equations introduced in [15]. For simplification, the source reflection coefficient is set to a predefined value Γ_S (Γ_{OPT}), Based on this assumption, the centre and radius of the OM circle can be calculated using the following equations:

$$Center = \frac{1 - OM^2}{1 - OM^2 \left|\Gamma_{OUT}\right|^2} \Gamma_{OUT*} \tag{7}$$

$$Radius = \frac{1 - \left|\Gamma_{OUT}\right|^2}{1 - OM^2 \left|\Gamma_{OUT}\right|^2} OM \tag{8}$$

Here OM = 0 represents a perfect match at output, which means $\Gamma_L = \Gamma_{OUT}*$; this is also equal to the centre of "OM = 0" circle. Similarly, IM = 0 circle can be obtained at $\Gamma_L = \Gamma_{LCin}$ which means perfect input match and can be evaluated from following equation:

$$\Gamma_{LCin} = \frac{(S_{11} - \Gamma_S *)}{(\Delta - \Gamma_S * S_{22})} \tag{9}$$

This equation is simply obtained by putting $\Gamma_S^* = \Gamma_{in}$ in Equation (3). This defines the centre of the IM = 0 circle on the Smith chart. To plot corresponding IM circles for various OM values, the following equations can be used:

$$Center = \frac{\Gamma_{LCin} - q^2 \Gamma_{OUT}^*}{1 - q^2 \, |\Gamma_{OUT}|^2} \tag{10}$$

$$Radius = \frac{1 - |\Gamma_{OUT}|^2}{1 - q^2 \, |\Gamma_{OUT}|^2} q \tag{11}$$

where the scaling factor (q) is defined as:

$$q = IM \left| \frac{1 - S_{11}\Gamma_s}{\Delta - S_{22}\Gamma_s^*} \right| \tag{12}$$

Using the equations described above and the IM-OM values listed in Table 1, the corresponding mismatch circles are plotted in Figure 4.

Table 1. OM values and corresponding IM Values.

OM (Linear)	0	0.1	0.25	0.3	0.6	0.65	0.7	0.8	0.895	0.952	1
OM [dB]	–∞	–20	−12	–10.46	–4.44	–3.74	–3.10	–1.94	−0.96	−0.43	0
IM (Linear)	0.47	0.36	0.3	0.25	0.1	0.08	0.05	0	0.05	0.08	0.1
IM [dB]	–6.56	–8.87	–10.46	–12	–20	–17.20	–20.90	–∞	−26	−21.9	−20

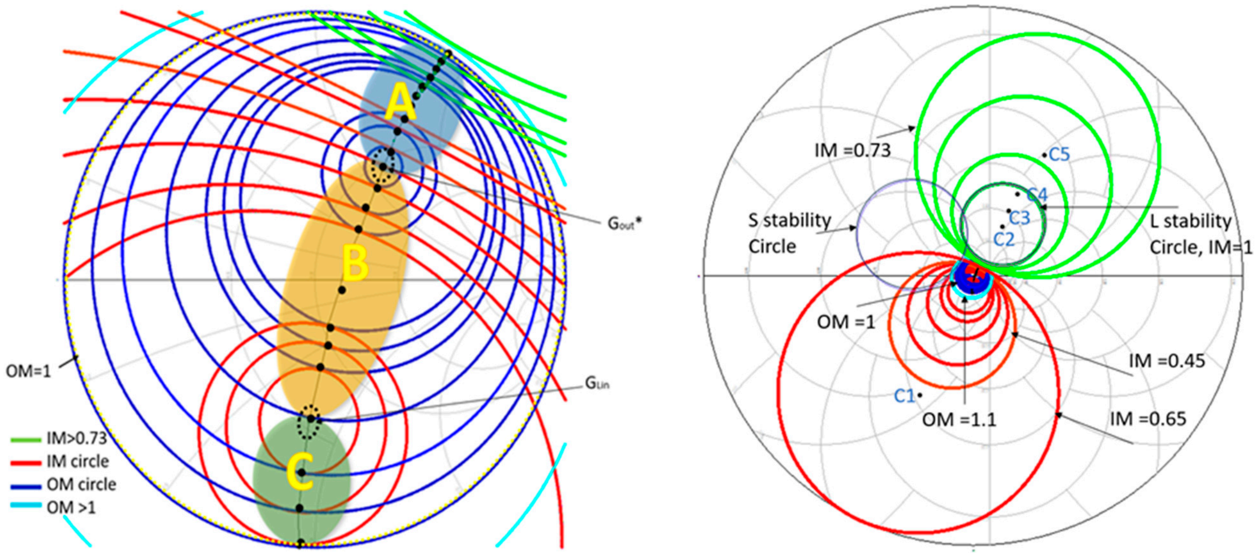

(**a**) (**b**)

Figure 4. (**a**) IM-OM circles (@31 GHz) for Ls = 70 pH; (**b**) IM-OM circles along with stability circles (zoomed out view).

As illustrated in Figure 4a, each IM or OM value corresponds to both a minimum and maximum counterpart; that is, every OM circle (blue) is associated with two potential IM values (red), and vice versa. The tangency points between these circles do not lie along a straight path but instead trace a curved trajectory, which becomes more noticeable as they move away from the centre of the Smith chart. Between the points $\Gamma_{OUT}{}^{*}$ and Γ_{Lin} no IM circle fully encloses an OM circle, and nor does any OM circle fully enclose an IM circle. Instead, these circles intersect at discrete points, forming a curved locus that defines Region B, a zone where the mismatch levels are balanced. By increasing the IM level further, IM circles begin to fully enclose OM circles, defining Region A. A similar reversal occurs in Region C, where elevated OM levels cause OM circles to enclose IM circles.

This dual behaviour demonstrates that, for any fixed OM, there exists both a minimum and maximum IM value, and vice versa, outlining a bounded range of feasible matching conditions. Notably, the OM = 1 circle aligns exactly with the boundary of the Smith chart (dotted black line), indicating $\Gamma_L = 1$, or a completely reactive load. The corresponding IM values for this OM = 1 condition are 0.1 and 0.9. When OM exceeds 1, the resulting circles completely encompass the Smith chart, reflecting load conditions with a negative real part. Such terminations imply instability and are therefore excluded from practical amplifier design.

Figure 4b presents a zoomed-out view of the IM and OM circles overlaid with the source and load stability circles. A notable behaviour observed in the IM circles (green) is their reversal of curvature direction after reaching a certain mismatch level. Specifically, in this process, the IM circles begin to reverse when IM ≈ 0.73, even before reaching the IM = 1 stability boundary. This curvature reversal originates from the shift in IM circle centres (e.g., C2, C3, C4, C5) into the right half of the Smith chart, which corresponds to active terminations. In this region, the device sees conditions conducive to instability, and the IM contour ceases to behave monotonically with respect to OM. This behaviour imposes a practical constraint on the maximum usable IM value in wideband amplifier design, especially when avoiding unstable terminations. The IM = 1 and OM = 1 contours also serve as stability boundaries, beyond which the device enters potentially unstable regions and thus is excluded. A linearised visualisation of the IM-OM tangency points discussed above is shown in Figure 5. The horizontal axis traces tangency points from the lower edge (point 1) to the upper edge (point 24) of the Smith chart.

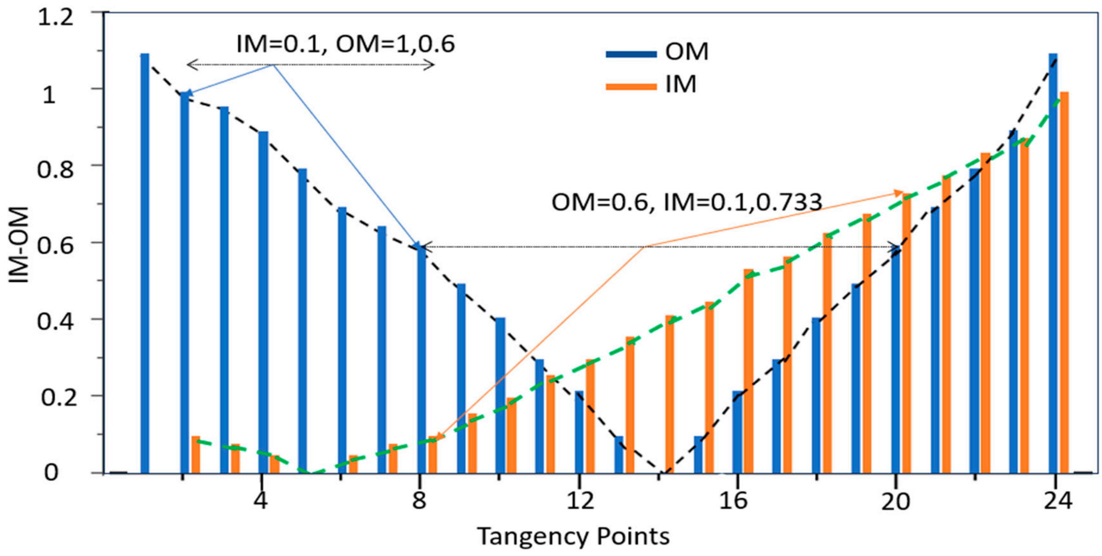

Figure 5. IM-OM pair with linear variation of tangency points shown in Figure 4 (moving from bottom (point 2) to top (point 24) of the Smith chart).

Point 1 represents an extreme case with OM = 1.1, indicating a highly mismatched and unstable load. Point 2 lies exactly on the OM = 1 circle and corresponds to IM = 0.1. Moving upward, point 5 intersects IM = 0, while point 14 marks OM = 0. At the final tangency point (point 24), the match reaches the IM = 1 circle, and OM again rises to 1.1, mirroring the behaviour observed at the chart's lower edge. In situations where only a single IM or OM value is observed, its alternate counterpart lies outside the unit Smith chart. These out-of-bound values represent either unstable or non-physical terminations and are excluded from practical use.

3.2. Frequency-Bounded Envelope of Various Mismatch Regions

The IM-OM circles introduced in Section 3.1 are extended to construct a frequency-bounded mismatch envelope on the Smith chart. This approach offers a structured graphical tool to select $\boldsymbol{\Gamma}_L$, based on relaxed SSNM conditions, for wideband LNA design.

The first step involves decomposing the operating frequency band into three discrete points (illustrated in Figure 6):

- f_1: Starting frequency of the band (29 GHz)
- f_2 (or f_0): Centre frequency (31 GHz)
- f_3: Ending frequency (33 GHz)

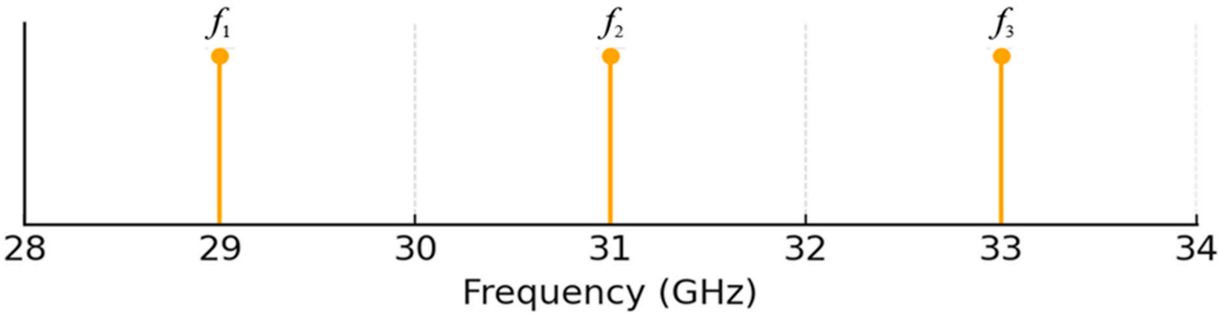

Figure 6. Frequency decomposition for wideband design (28–34 GHz).

The second step is the selection of appropriate source reflection coefficients $\boldsymbol{\Gamma}_S$ at the three chosen frequencies:

- $\boldsymbol{\Gamma}_{S1} = \boldsymbol{\Gamma}_{OPT}$ @ 29 GHz
- $\boldsymbol{\Gamma}_{S2} = \boldsymbol{\Gamma}_{OPT}$ @ 31 GHz
- $\boldsymbol{\Gamma}_{S3} = \boldsymbol{\Gamma}_{OPT}$ @ 33 GHz

In the third step, the independent sets of IM and OM circles at each frequency are generated using the equations defined in Section 3.1 and using $\boldsymbol{\Gamma}_S$ values defined in step 2. The fourth step involves tracing the loci of tangency points between the IM and OM circles for all three frequencies. These points define the practical IM-OM pairs across the band. The lower tangency points from f_1 to f_3 are connected to form the lower boundary, and the upper tangency points define the upper boundary of the frequency-bounded mismatch region. As shown in Figure 7a, the left and right edges of the envelope correspond to tangency points at f_1 and $f_{3,}$ respectively.

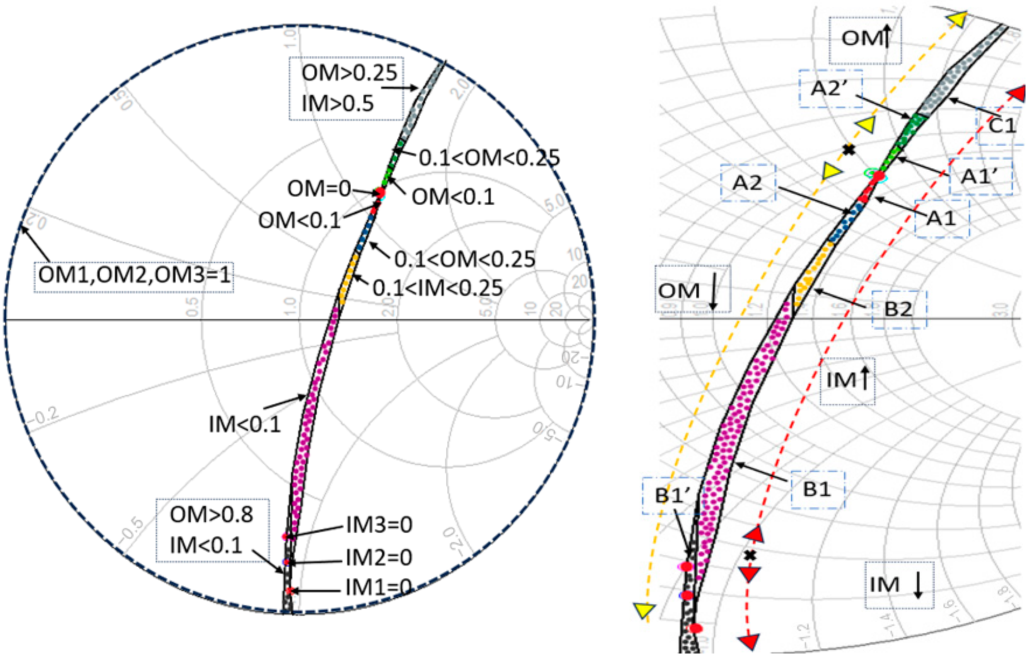

(**a**) (**b**)

Figure 7. (**a**) Frequency-bounded mismatch region, formed using tangency loci at f_1, f_2, and f_3; (**b**) categorised mismatch zones based on IM and OM levels.

The interior of the envelope shown in Figure 7a is subdivided into several mismatch zones (Figure 7b), which guide the selection of appropriate reflection coefficients for each stage of the LNA.

1. Low mismatch zones
   - A1: $0 < |\text{OM}| < 0.1$ (red shaded area)
     This region is suitable for designing the last stage, or in between stages, where strong output matching is critical and a higher gain is desired. It typically offers output return loss better than −20 dB. However, the input mismatch in this region may be higher.
   - A1′: $0 < |\text{OM}| < 0.1$ (light green shaded area)
     This region lies opposite side of A1, with $\Gamma_{OUT}{}^{*}$ being the centre. In this region, OM is the same, but IM is comparatively larger than A1. It may be useful for inter stages focused on good S_{22} performance.
   - B1: $0 < |\text{IM}| < 0.1$ (pink shaded area)
     Similar to A1, this zone supports input matching with excellent return loss. In this region, OM is higher. This region can be used to design the initial stages.
   - B1′: $0 < |\text{IM}| < 0.1$ (black shaded area)
     This represents the mirrored region of B1, with excellent IM but much higher OM. It is suitable for stages where input reflection dominates performance considerations.
2. Acceptable mismatch zones
   - A2: $0.1 < |\text{OM}| < 0.25$ (blue shaded area)
   - Represents a more relaxed output match. It can be used where −12 dB to −20 dB return loss is sufficient. In this region, IM is higher than OM but lower than the A1 region.
   - A2′: $0.1 < |\text{OM}| < 0.25$ (green shaded area)
   - This region has the same output mismatch as A2, but IM is comparatively higher than A2 and A1.

- B2: 0.1 < |IM| < 0.25 (yellow shaded area)
  It is similar to A2; in this region, IM remains in an acceptable range. These regions are suitable for intermediate stages where a balance between input and output matching is acceptable, and design constraints are less strict.

3. High mismatch zone
   - C1: Corresponds to areas where mismatch exceeds its largest possible limits. These regions may be avoided in critical input–output paths but are occasionally useful in buffering stages or gain shaping.

It is important to note that the specific shape and distribution of these regions depend on the transistor model, bias conditions, and technology. Additional mismatch zones may emerge for other configurations. For example, moderate mismatch regions with both IM and OM exceeding 0.25 may form separate sub-regions. However, for the device studied in this work, such regions overlap significantly with A2 and B2 due to the inherent convergence of IM-OM boundaries.

This analysis confirms that the frequency-bounded mismatch map is flexible, scalable, and adaptable to both wideband and narrowband amplifier designs. The categorised zones serve as a visual aid for selecting suitable $\boldsymbol{\Gamma}_\mathrm{L}$ values that meet relaxed SSNM constraints across multiple stages, thereby streamlining the design process and minimising reliance on iterative optimisation. Furthermore, this method extends naturally to much wider bandwidths. The construction procedure remains unchanged: the mismatch envelope is primarily defined by the tangency loci at the start and end of the band. Additional intermediate frequencies may be used to refine the internal structure of the envelope and improve the resolution between regions, especially in ultra-wideband designs. This generalisation makes the approach suitable for a broad range of RF and mm-wave applications with stringent bandwidth requirements.

4. Wideband LNA Design Strategy Using Modified SSNM Conditions

A wideband design strategy is developed in this paper using relaxed SSNM conditions and frequency-bounded envelopes. The first step in wideband implementation, which is the focus of this work, involves decomposing the operating frequency band into discrete frequency points. For this study, a three-point decomposition is employed, as described in Section 3.2. While additional frequency points may improve accuracy, they also increase computational complexity.

The second step is to select the proper size of the transistor and bias conditions based on the required noise figure and available gain. Subsequently, the appropriate L_S for each stage is determined using mismatch charts (see Figures 2 and 3). The goal is to locate stable operating regions that satisfy gain–noise trade-offs and remain within the relaxed mismatch bounds. L_{S1} = 70 pH, L_{S2} = 60 pH and L_{S3} = 70 pH was selected with gate bias voltages of 0.6 V, 0.65 V, and 0.7 V for stages 1, 2, and 3, respectively. The drain voltage (Vds) was set to 1.2 V for all stages.

Next, it is necessary to define the design targets for each stage and synthesise the corresponding matching networks. This starts with synthesising the input matching network (IMN) of the first stage, as introducing input mismatch does not significantly impact its design. Following this, the output matching network (OMN) of the last stage is synthesised, which can be designed with or without deliberate mismatch, depending on the desired performance trade-offs.

1. First stage: Minimum noise figure—IMN synthesis

The total noise figure (NF_{CAS}) of a cascaded system is given by Friis' formula [26]:

$$NF_{CAS} = NF1 + \frac{NF2 - 1}{G1} + \frac{NF2 - 1}{G1G2} + \ldots\ldots \tag{13}$$

This expression highlights the predominant influence of the first-stage noise figure on overall system performance. However, the contribution of further stages can be understood by the available gain from each stage. Haus and Adler [27] introduced the noise measure (M) as a quantity to give an idea about the quality of the overall noise figure of a cascaded network.

$$M = \frac{F - 1}{1 - \frac{1}{G}} \tag{14}$$

where F is the noise factor and G is the available gain. Minimising the overall noise figure requires "$M_{N-1} < M_N$" across stages [28].

To synthesise IMN for minimum noise, we select three Γ_S values as follows: $\Gamma_{S11} = \Gamma_{OPT}\ @\ f_1$, $\Gamma_{S12} = \Gamma_{OPT}\ @\ f_2$, and $\Gamma_{S13} = \Gamma_{OPT}\ @\ f_3$; match these three points to 50 Ω. This typically requires multiple matching elements instead of the classic two elements. We then introduce a deliberate mismatch at the first stage output, selecting a suitable Γ_{L1ref} from mismatch region B1 or B2 (Figure 7b) and obtaining the corresponding OM values.

2. Last stage: Maximum gain—OMN synthesis

Instead of designing a second stage after the first one, the parameters of the third stage that yield the maximum gain are decided. Therefore, it is necessary to choose appropriate Γ_{S3ref} for the third stage (ex., can be a point for max gain from constant gain circles) and select an appropriate mismatch, similar to the first stage. The procedure. Following this is then to choose a reference Γ_{L3ref} from the mismatch region A1 or A2 and synthesize an output matching network to match the Γ_{L31}, Γ_{L32}, Γ_{L33} to Γ_{L3ref} value.

3. Middle stage: Relaxed SSNM based determination

The middle stage is not directly designed to match 50 Ω; instead:

- Derive its matching conditions from neighbouring stages via relaxed SSNM.
- Use mismatch transfer theory (lossless matching networks preserve reflection coefficients)

Choose a Γ_{S2ref} and Γ_{L2ref} value for a trade-off between gain and noise.

3.1. ISMN1: OM1 ≈ IM2

To synthesise the first inter-stage matching network (ISMN1), we first ensure that the output mismatch of stage 1 equals the input mismatch of Stage 2. Then ISMN1 is designed in such a way that input reflection coefficients (Γ_{L11}, Γ_{L12}, Γ_{L13}) at f_1, f_2, and f_3 at port1 of ISMN1 are equal to or in the vicinity of Γ_{L1ref} (derived from the output of the first stage) as shown in Figure 8. Similarly, the output port of ISMN1 (Γ_{S21}, Γ_{S22}, Γ_{S23}) is simultaneously matched at these three frequencies to Γ_{S2ref}, specified at the input of the second stage. This ensures consistent and optimised mismatch transfer across the entire targeted frequency band. To further simplify ISMN1, we can match Γ_{S23} of ISMN1 to Γ_{S2ref} value, as we obtain maximum NF at high frequencies and doing this would not increase the NF beyond the overall limit of the noise figure.

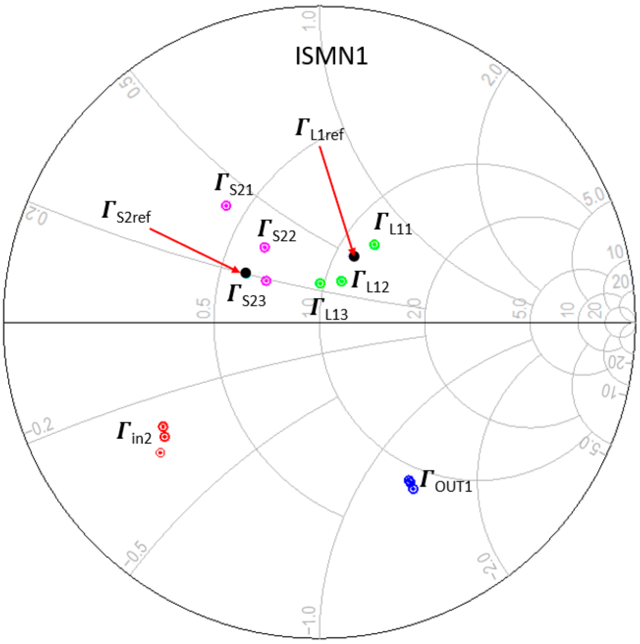

Figure 8. Smith chart representation of various reflection coefficients for ISMN1.

3.2. ISMN2: OM2 ≈ IM3

To synthesise the second inter-stage matching network (ISMN2), again, it is necessary to enforce the relaxed matching condition. The input port of ISMN2, looking into the matching network, is matched at the three frequency points to the reference load reflection coefficients derived from the output of the second stage. Similarly, the output side of ISMN2 is simultaneously matched at these frequencies to the reference source reflection coefficients specified at the input of the third stage. Figure 9 depicts the matching conditions for the ISMN2.

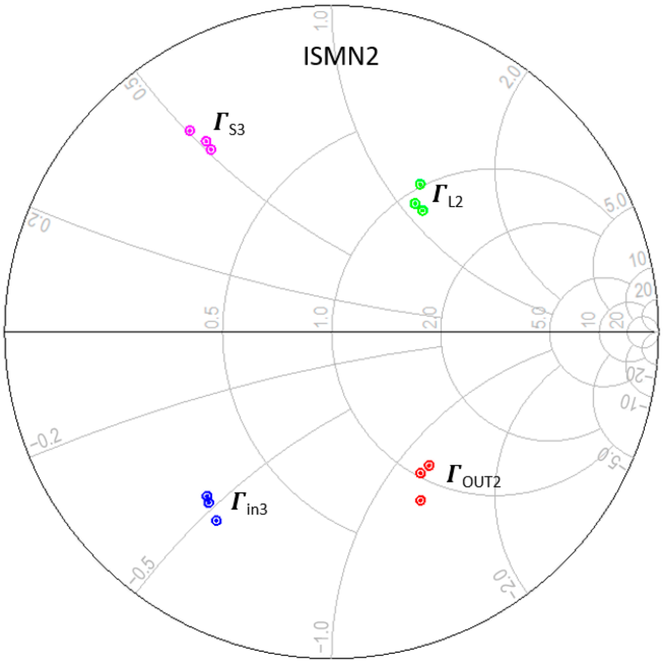

Figure 9. Smith chart representation of reflection coefficients for ISMN2.

Complementing these visualisations (Figures 8 and 9), Table 2 summarises the corresponding IM and OM values obtained at these frequencies.

Table 2. IM-OM values at three frequencies for three stages.

	IM (f_1)	IM (f_2)	IM (f_3)	OM (f_1)	OM (f_2)	OM (f_3)
Stage1	0.10	0.067	0.072	0.270	0.401	0.442
Stage2	0.253	0.384	0.42	0.052	0.038	0.038
Stage3	0.070	0.051	0.047	0.148	0.091	0.123

The corresponding S-parameters of the designed MMIC using lossless components are shown in Figure 10.

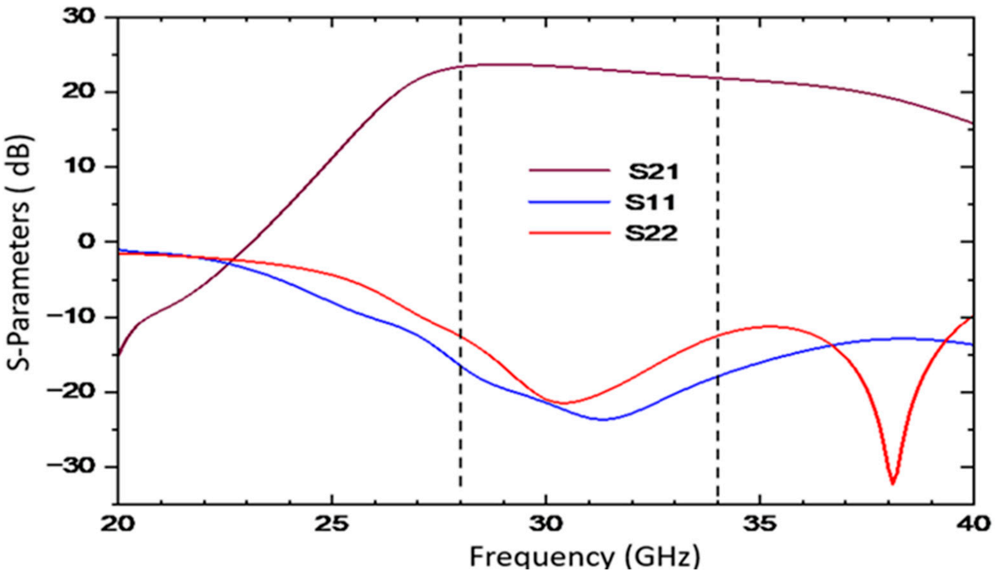

Figure 10. S-parameter vs. frequency of 3-stage LNA with lossless transmission lines.

These combined charts and numerical values confirm that the proposed relaxed SSNM framework effectively guides the wideband MMIC design by providing practical, frequency-dependent reflection coefficient targets that maintain stable and efficient operation throughout the desired frequency range.

This entire strategy to design a wideband matching network is summarised in the flow chart shown in Figure 11:

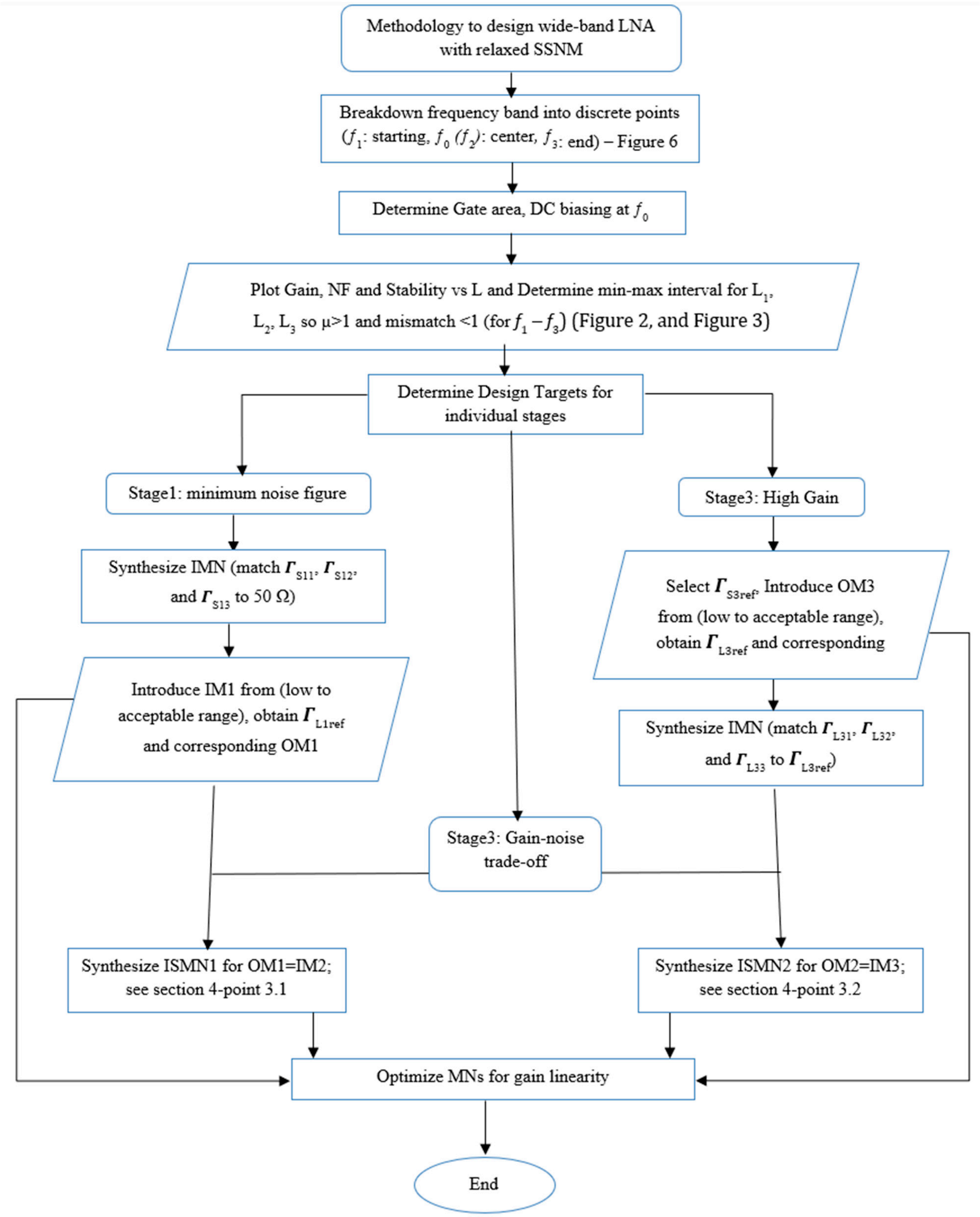

Figure 11. Design-methodology flow chart for a three-stage LNA MMIC.

5. MMIC Implementation

To demonstrate the practical application of the relaxed SSNM condition and the design strategy outlined in Section 3, a three-stage LNA MMIC operating in the Ka-band (28–34 GHz) was designed. The circuit structure, shown in Figure 12, utilised ideal microstrip lines initially, which were then replaced by equivalent components available in the WIN PQ07-0C GaAs process. The PQ07-0C process, provided by WIN, features 0.15 µm GaAs PHEMT transistors available in both E-mode and D-mode. E-mode HEMTs are optimised for single-supply LNAs and PAs, whereas D-mode devices are primarily intended for PA and switch applications. Reliability testing recommends operating the PQ07-0C process at 4 V. Deep UV lithography enables the fabrication of high-voltage f_T transistors suitable for various markets and applications. The process supports two metal layers, dielectric crossovers, precision resistors (50 Ω/sq and >4 kΩ/sq), PN diodes for electrostatic discharge (ESD) protection, and options for high-performance packaging, including hot vias and Cu-pillar bumps. These features contribute to a moisture-robust platform.

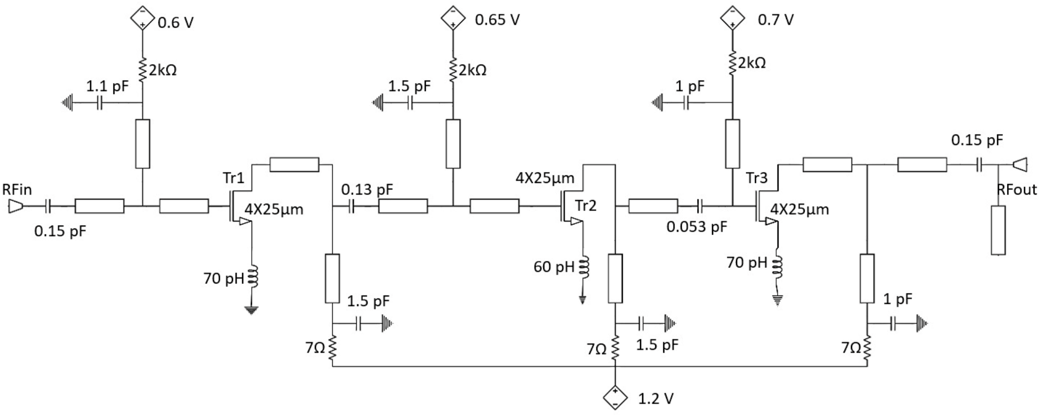

Figure 12. Circuit schematic of the three-stage wideband LNA MMIC showing transistor sizes, biasing, and matching elements.

Source degeneration inductors, shown in Figure 12, were replaced with equivalent transmission line models provided by the foundry. This approach helps reduce the area and unwanted parasitic losses, while still achieving the desired feedback performance.

For this LNA MMIC, E-mode PHEMT transistors with a gate geometry of 4 × 25 µm were selected due to their low noise figure characteristics. The first two stages are optimised for minimum noise and biased with gate voltages of 0.6 V and 0.65 V, respectively. The third stage is designed for high gain, with a gate bias set to 0.7 V.

Figure 13 shows a microphotograph of the fabricated MMIC chip. The layout adheres to best practice for mm-wave design in the 0.15 µm GaAs process, featuring compact transistor placement, carefully routed matching networks, and well-designed RF input/output pads for on-wafer probing. The chip footprint measures approximately 2.5 × 3.4 mm^2, demonstrating the integration of the wideband relaxed SSNM design approach in a practical MMIC.

The MMIC's performance was evaluated under the specified biasing conditions to ensure it met the design goals and aligned with simulation results. On-wafer S-parameter measurements were performed across the 20 to 40 GHz frequency range with 100 MHz increments, utilizing an HP8510C Vector Network Analyzer. Calibration of the measurement setup was carried out using the standard Short-Open-Load-Thru (SOLT) technique. For noise figure characterization, an Agilent E4448A Spectrum Analyzer was used, with the noise signal amplified beforehand by two low-noise amplifiers: a MACOM MAAM-011109 and an HP83051A. Measured outputs of the MMIC are presented in the following section.

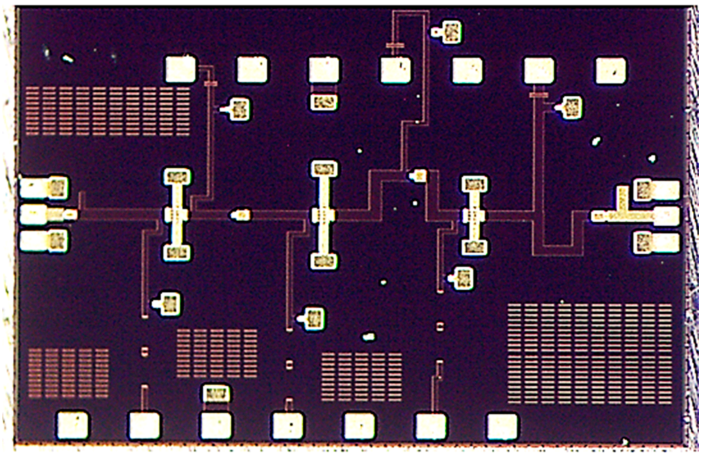

Figure 13. Microphotograph of the fabricated three-stage LNA MMIC implemented in 0.15 μm GaAs technology.

6. Results and Discussion

The designed MMIC prototype was realised and measured for the 20 to 40 GHz frequency band. To validate small-signal stability across the operating band, the fabricated MMIC LNA was subjected to a comprehensive analysis using multiple standard and advanced criteria. Figure 14 shows the computed Rollet stability factor (K) and geometrical stability factors, which confirm unconditional stability across the frequency range of DC to 70 GHz with both μ and K exceeding unity.

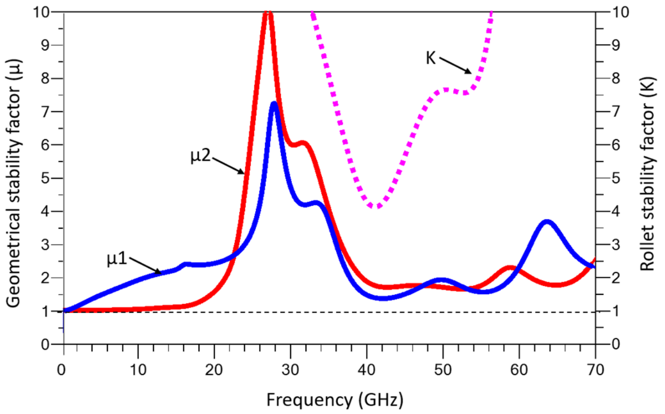

Figure 14. Simulated Rollet stability factor (K) and graphical stability factors (μ_1, μ_2) of the LNA across 0–70 GHz, confirming unconditional small-signal stability.

In addition, the partitioned Ohtomo stability test was applied to all ports of the three-transistor cascade using the methodology proposed in [29]. The Ohtomo test provides a powerful framework to detect internal feedback-induced instability by evaluating each terminal's reflection behaviour on a Smith chart. The corresponding six Ohtomo circle plots are shown in Figure 15, with each subplot corresponding to one of the six transistor terminals.

The plots confirm that the trajectories do not encircle or approach the instability boundary ((1,0) point at x-axis), indicating that no unstable pole exists for any terminal across the frequency sweep. This confirms that all transistor stages remain unconditionally stable, even when mismatches and interstage feedback are present. The test thus validates the core premise of this work, that relaxing the SSNM condition does not compromise stability.

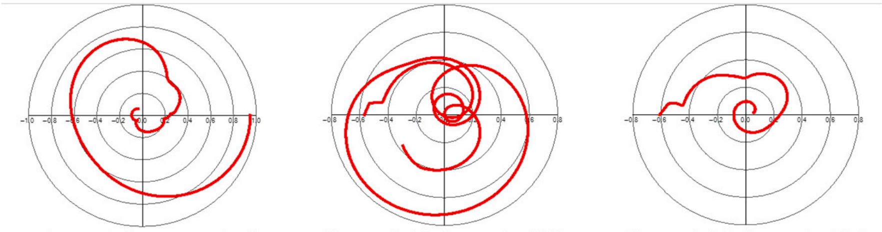

Ohtomo circle1: Gate node of Tr1 Ohtomo circle2: Gate node of Tr2 Ohtomo circle3: Gate node of Tr3

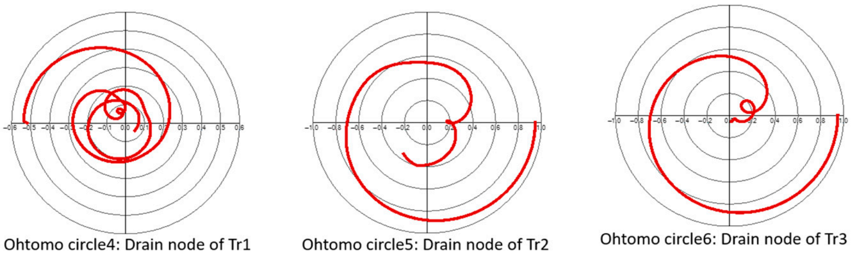

Ohtomo circle4: Drain node of Tr1 Ohtomo circle5: Drain node of Tr2 Ohtomo circle6: Drain node of Tr3

Figure 15. Partitioned Ohtomo test results for each terminal of the three-stage LNA MMIC (DC to 70 GHz).

Figure 16 presents both simulated and measured S-parameters (in dB) alongside the noise figure of the proposed three-stage LNA. Across the targeted 28–34 GHz frequency band, the amplifier achieves a flat and stable gain of approximately 23 ± 1 dB, with measured gain closely following simulation predictions. The simulated NF, shown as a solid magenta curve, remains below 2 dB throughout the operating band. The measured NF, depicted by the dashed magenta line, varies between 2.0 dB to 2.5 dB over 28 to 34 GHz.

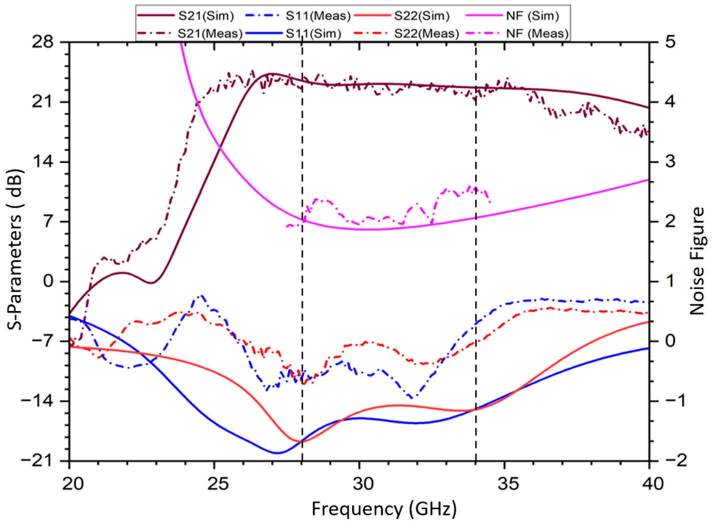

Figure 16. Simulated (post EM) and measured S-parameters and noise figure of the LNA MMIC.

As depicted in Figure 16, the simulated reflection coefficients (S11 and S22) demonstrate excellent wideband matching, maintaining better than −18 dB and −15 dB return loss, respectively, over the 28–34 GHz band. This broad matching performance directly validates the effectiveness of the relaxed SSNM design approach, which expands the permissible mismatch regions to achieve robust wideband impedance control.

While minor deviations between simulated and measured S11 and S22 occur, primarily due to parasitic effects such as probe pad capacitances, calibration inaccuracies, and small process variations, these measurement variations are independent of the relaxed SSNM condition itself. A similar variation occurs in the noise figure, which shows a noise figure increment of 0.5 dB at some frequencies; this is due to the difference between the noise model and noise data provided by the foundry.

Thus, the relaxed SSNM methodology inherently enables wideband operation, and the observed differences in measured data stem from practical implementation factors rather than the design approach, confirming the method's practical reliability and wideband applicability.

A comparison with previously published LNA MMICs, fabricated using the same GaAs technology, is summarised in Table 3. As observed, the performance of the proposed design is comparable to, or better than existing designs. References [8,10,11,18,21,30] all utilize transistors with a 150 nm gate length, similar to that used in this work. However, reference [8] shows a high noise figure and a high gain due to a bigger transistor size. Reference [10] demonstrates excellent performance, and [11,18] achieve comparable results. All three LNAs operate for ultra-wideband but rely on extra circuitry. References [21,30] report a significantly higher noise figure, despite employing only two amplifier stages. Additionally, none of the referenced works provides a systematic methodology for achieving wideband performance. Instead, they depend heavily on additional circuitry or extensive software-based optimisation. In contrast, the proposed approach offers a structured and efficient alternative, achieving competitive performance without the need for extra circuitry.

Table 3. State-of-the-art GaAs LNA MMICs in Ka-band.

Ref No.	BW (GHz)	Channel Width (nm)	Gate Geometry (Fingers × Width (um))	No. of Stages	S21 (dB)	S11, S22 (dB)	NF (dB)	Topology
[3]	26–36	100	2 × 50	4	33	−12, −12	1.8	Grounded FET
[8]	25–35	150	4 × 120	3	28	−10, −15	3	Source degeneration
[9]	27–31	70	4 × 30	3	26	−10, −10	1.6	Source degeneration
[10]	14–31	150	2 × 50, 1 × 50	4	30–25	−10, −10	1.25	Drain-gate RLC feedback
[11]	27-34	250	Not avai.	5	30	Not avai.	2-3	Grounded FET
[12]	18.7–36.5	100	4 × (25, 75)	2	15.9	−10, −10	1.5–2.1	R-L-C feedback
[13]	18–43	100	4 × (25, 35, 50)	3	21.6	−10, −10	1.8–2.7	Feedback
[18]	13–33	150	6 × 40	3	15.6–18.6	−8, −10	1.05–2.8	R-L-C shunt feedback
[19]	11–39	100	4 × 25	3	23	−2, −10	2.1–3	Transformer feedback
[20]	27–31	100	Not avai.	3	20	−12, −12	1.6	Filtering matching networks
[21]	29–44	150	Not avai.	2	14.2	−10, −7	2.3–3	Forward combining
[30]	27–34	150	Not avai.	2	22.9	−10, −10	2.7–3.2	Cascode, CS
This work	28–34	150	4 × 25 µm	3	24 ± 1	−10, −11	2–2.5	Source degeneration

7. Conclusions

This work extends the classical SSNM concept from narrowband theory to practical wideband application by introducing deliberate mismatches at the external ports; thus, it removes ambiguity in inter-stage mismatch levels. Each stage can function inside a frequency-bounded mismatch envelope described by IM-OM circles (derived from closed-form equations in the literature). Thanks to the relaxed SSNM conditions, the proposed graphical charts guide the designer across the entire band, while preserving an improved balance among gain, noise figure, and stability.

An easy-to-follow strategy for wideband implementation using the relaxed SSNM condition is presented, supported by an MMIC demonstration. This approach significantly limits reliance on CAD-based optimisation when targeting wide frequency bands. The fabricated MMIC prototype achieves over 23 dB gain and 2–2.5 dB noise figure, from 28 GHz to 34 GHz, with measured results closely tracking simulations.

The methodology naturally scales to wider bandwidths without modification and extends to N-stage cascaded LNAs. The improved IM-OM versus L_S charts with induced mismatch scale provide a practical tool for selecting source degeneration inductors across multiple stages, and the frequency-bounded mismatch regions can be adapted for broader frequency spans.

Future Work Directions

Future work will focus on integrating the envelope construction into an automated synthesis engine and validating the method across octave-band LNAs and reconfigurable front-ends. This will help transform the relaxed SSNM concept into a wideband design framework suitable for next-generation microwave and millimetre-wave systems. Further studies will explore mismatch limits over varying frequency bands. These efforts will broaden the applicability of the approach and ultimately make it more accessible to diverse real-world design scenarios.

Author Contributions: Conceptualization, V.S. and P.E.L.; methodology, V.S.; software, V.S. and S.S.; validation, W.C., S.C. and A.S.; formal analysis, V.S. and P.E.L.; investigation, W.C., S.C. and A.S.; resources, P.E.L. and E.L.; data curation, V.S., S.S. and P.E.L.; writing—original draft preparation, V.S.; writing—review and editing, V.S., S.S. and P.E.L.; visualization, V.S. and S.S.; supervision, P.E.L. and E.L.; project administration, P.E.L. and E.L.; funding acquisition, E.L. All authors have read and agreed to the published version of the manuscript.

Funding: This research received no external funding.

Institutional Review Board Statement: Not applicable.

Informed Consent Statement: Not applicable.

Data Availability Statement: Data are contained within the article.

Acknowledgments: The MMIC described in this work was fabricated using the PQG3-0C technology provided by WIN Semiconductors as part of the “select university” program for the Microwave Engineering Center for Space Applications (MECSA). The authors express their sincere gratitude to David Danzilio and the WIN Customer Engineering Department for their invaluable support. They also thank Filippo Bolli and Enzo De Angelis for their assistance in characterising the low-noise amplifier. The authors have reviewed and edited the output and take full responsibility for the content of this publication.

Conflicts of Interest: The authors declare no conflicts of interest.

References

1. Huang, C.; Zhang, Z.; Wang, X.; Liu, H.; Zhang, G. An MMIC LNA for Millimeter-Wave Radar and 5G Applications with GaN-on-SiC Technology. *Sensors* **2023**, *23*, 6611. [CrossRef] [PubMed]
2. Li, F.; Wu, Y. Ka-band Single-chip GaAs PHEMT Transceiver MMIC for Ranging FMCW Radar. In Proceedings of the 2019 International Conference on Microwave and Millimeter Wave Technology (ICMMT), Guangzhou, China, 19–22 May 2019; pp. 1–3. [CrossRef]

3. Cuadrado-Calle, D.; George, D.; Fuller, G. A GaAs Ka-band (26–36 GHz) LNA for radio astronomy. In Proceedings of the 2014 IEEE International Microwave and RF Conference (IMaRC), Bangalore, India, 15–17 December 2014; pp. 301–303. [CrossRef]
4. Ciccognani, W.; Longhi, P.E.; Colangeli, S.; Limiti, E.; Senior Member IEEE. Q/V band LNA for satellite on-board space applications using a 70 nanometers GaAs mHEMT commercial technology. *Microw. Opt. Technol. Lett.* **2018**, *60*, 2185–2190. [CrossRef]
5. Arican, G.O.; Akcam, N.; Yazgan, E. Ku-Band MMIC LNA Design for Space Applications. In Proceedings of the 2019 6th International Conference on Electrical and Electronics Engineering (ICEEE), Istanbul, Turkey, 16–17 April 2019; pp. 274–278. [CrossRef]
6. Jung, S.-J.; Hong, S.-K.; Kwon, O.-K. Low-Power Low-Noise Amplifier Using Attenuation-Adaptive Noise Control for Ultrasound Imaging Systems. *IEEE Trans. Biomed. Circuits Syst.* **2017**, *11*, 108–116. [CrossRef] [PubMed]
7. Teo, T.H.; Yeoh, W.G. Low-Power Short-Range Radio CMOS Subharmonic RF Front-End Using CG-CS LNA. In *IEEE Transactions on Circuits and Systems II: Express Briefs*; IEEE: Piscataway, NJ, USA, 2008; Volume 55, pp. 658–662. [CrossRef]
8. Chou, H.-S.; Liu, C.-C.; Chen, T.H. Ka-band monolithic GaAs PHEMT low noise and driver amplifiers. In Proceedings of the APMC 2001. 2001 Asia-Pacific Microwave Conference (Cat. No.01TH8577), Taipei, Taiwan, 3–6 December 2001; Volume 1, pp. 139–142. [CrossRef]
9. Sharma, S.; Colangeli, S.; Longhi, P.; Ciccognani, W.; Serino, A.; Limiti, E. A Ka-Band Ultra-Low Power GaAs MMIC LNA. In Proceedings of the SIE 2023, Rende, Italy, 5–7 September 2023; Lecture Notes in Electrical Engineering. Ciofi, C., Limiti, E., Eds.; Springer: Cham, Switzerland, 2024; Volume 1113. [CrossRef]
10. DNguyen, P.; Pham, B.L.; Pham, T.; Pham, A.-V. A 14–31 GHz 1.25 dB NF enhancement mode GaAs pHEMT low noise amplifier. In Proceedings of the 2017 IEEE MTT-S International Microwave Symposium (IMS), Honolulu, HI, USA, 4–9 June 2017; pp. 1961–1964. [CrossRef]
11. Feng, M.; Scherrer, D.; Apostolakis, P.; Middleton, J.; McPartlin, M.; Lautenvasser, B.; Oliver, J. Ka-band monolithic low-noise amplifier using direct ion-implanted GaAs MESFETs. *IEEE Microw. Guid. Wave Lett.* **1995**, *5*, 156–158. [CrossRef]
12. Nikandish, G.; Medi, A. Transformer-Feedback Interstage Bandwidth Enhancement for MMIC Multistage Amplifiers. *IEEE Trans. Microw. Theory Tech.* **2015**, *63*, 441–448. [CrossRef]
13. Sabzi, M.; Medi, A. Analysis and design of multi-stage wideband LNA using simultaneously noise and impedance matching method. *Microelectron. J.* **2019**, *86*, 97–104, ISSN 1879-2391. [CrossRef]
14. Longhi, P.E.; Pace, L.; Colangeli, S.; Ciccognani, W.; Limiti, E. Novel Design Charts for Optimum Source Degeneration Tradeoff in Conjugately Matched Multistage Low-Noise Amplifiers. *IEEE Trans. Microw. Theory Tech.* **2021**, *69*, 2531–2540. [CrossRef]
15. Ciccognani, W.; Longhi, P.E.; Colangeli, S.; Limiti, E. Constant Mismatch Circles and Application to Low-Noise Microwave Amplifier Design. *IEEE Trans. Microw. Theory Tech.* **2013**, *61*, 4154–4167. [CrossRef]
16. Abdalrahman, F.; Longhi, P.E.; Colangeli, S.; Ciccognani, W.; Serino, A.; Limiti, E. Insight into Optimally Noise- and Signal-Matched Three-Stage LNAs and Effect of Inter-Stage Mismatch. *Electronics* **2025**, *14*, 1967. [CrossRef]
17. Albinsson, B.M. A graphic design method for matched low-noise amplifiers. *IEEE Trans. Microw. Theory Tech.* **1990**, *38*, 118–122. [CrossRef]
18. Hwang, S.; Kang, D.; Lee, Y.; Park, D.-W. A 13–33 GHz Wideband Low-Noise Amplifier in 150-nm GaAs Based on Simultaneous Noise- and Input-Matched Gain-Core with R-L-C Shunt Feedback Network. *Electronics* **2025**, *14*, 450. [CrossRef]
19. Nikandish, G.; Yousefi, A.; Kalantari, M. A Broadband Multistage LNA With Bandwidth and Linearity Enhancement. *IEEE Microw. Wirel. Compon. Lett.* **2016**, *26*, 834–836. [CrossRef]
20. Armengaud, V.; Lintignat, J.; Barelaud, B.; Jarry, B.; Babak, L.I.; Laporte, C. Design of a Ka-band MMIC filtering LNA with a metamorphic HEMT technology for a space application. In Proceedings of the 2008 European Microwave Conference, Amsterdam, The Netherlands, 27–31 October 2008; pp. 1358–1361. [CrossRef]
21. Yu, Y.H.; Hsu, W.H.; Chen, Y.J.E. A ka-band low noise amplifier using forward combining technique. *IEEE Microw. Wirel. Compon. Lett.* **2010**, *20*, 672–674. [CrossRef]
22. Ahn, H.; Ji, H.; Kang, D.; Son, S.-M.; Lee, S.; Han, J. A 26–30 GHz GaN HEMT Low-Noise Amplifier Employing a Series Inductor-Based Stability Enhancement Technique. *Electronics* **2022**, *11*, 2716. [CrossRef]
23. Mao, F.; Chen, Z.; Li, B.; Wu, Z.; Chen, X.; Guan, Q. A 23–29 GHz GaN Low-Noise Amplifier with Drain-to-Source Coupling Feedback. *Electronics* **2024**, *13*, 4154. [CrossRef]
24. Güneş, F.; Demirel, S.; Özkaya, U. A low-noise amplifier design using the performance limitations of a microwave transistor for the ultra-wideband applications. *Int. J. RF Microw. Comput. Aided Eng.* **2010**, *20*, 535–545. [CrossRef]
25. Ciccognani, W.; Colangeli, S.; Longhi, P.E.; Serino, A.; Giofre, R.; Pace, L.; Limiti, E. Broadband Amplifier Design Technique by Dissipative Matching Networks. In *IEEE Transactions on Circuits and Systems I: Regular Papers*; IEEE: Piscataway, NJ, USA, 2021; Volume 68, pp. 148–160. [CrossRef]
26. Pozar, D.M. *Microwave Engineering: Theory and Techniques*; John Wiley & Sons: Hoboken, NJ, USA, 2021.
27. Haus, H.A.; Adler, R.B. Optimum Noise Performance of Linear Amplifiers. *Proc. IRE* **1958**, *46*, 1517–1533. [CrossRef]

28. Engberg, J.; Gawler, G. Significance of the Noise Measure for Cascaded Stages. *IEEE Trans. Circuit Theory* **1969**, *16*, 259–260. [CrossRef]
29. Colangeli, S.; Pantoli, L.; Ciccognani, W.; Longhi, P.E.; Leuzzi, G.; Limiti, E. Partitioned Ohtomo Stability Test for Efficient Analysis of Large-Signal Solutions. *IEEE Access* **2024**, *12*, 52227–52236. [CrossRef]
30. Su, Y.-C.; Huang, K.-H.; Chang, H.-Y. A Ka-Band Low Noise Amplifier Using R-L-C Feedback Technique in E-Mode 0.15-µm GaAs pHEMT Process. In Proceedings of the 2024 IEEE Asia-Pacific Microwave Conference (APMC), Bali, Indonesia, 17–20 November 2024; pp. 1165–1167. [CrossRef]